Supplementary Materials (ESI) for Journal of Marerials Chemistry A

Cutting off the upstream and downstream costs for CO_2 electroreduction by upcycling fermentation emissions into ethanol

Ruofan Sun,[1,2†] Jiwu Zhao,[1,2†] Xu Lu[1,2*]

[1] CCRC, Division of Physical Science and Engineering (PSE), King Abdullah University of Science and Technology (KAUST), Thuwal, 23955-6900, Kingdom of Saudi Arabia.

[2] KAUST Solar Center (KSC), PSE, KAUST.

† These authors contributed equally.

* Corresponding author. Email: Xu Lu (xu.lu@kaust.edu.sa).

Experimental

Fermentation broth. 0.1 M glucose solutions with different electrolytes (0.5 M KCl, 0.5 M $KHCO_3$ and 0.5 M K_2CO_3) were prepared as the fermentation feedstock. 5 g of active yeast (Victoria) was added into 250 mL of the fermentation feedstock at room temperature. Fermentation emissions were analyzed by GC (Trace 1310, Thermo Scientific) equipped with Molecular Sieve 5A and Porapak columns.

Electrode preparation. The tandem electrodes were fabricated by a four-step procedure. First, a carbon paper substrate (Toray 120, Fuel Cell Store, 0.30 mm thick) was subjected to electron-beam deposition (Denton Vacuum, LLC) to deposit a layer of 500 nm thick silver at a deposition rate of 0.2 nm s^{-1}. Subsequently, we manufactured paper-based shadow masks with varying interface numbers by CO_2 laser cutting (VLS 3.50 Laser 10.6 μm) in vector mode. Using the masks, a 1000 nm thick copper layer was deposited onto the substrate using electron-beam deposition (Denton Vacuum, LLC) at a deposition rate of 0.2 nm s^{-1}. At last, electrochemical oxidation of copper was performed in 1 M NaOH solution at a constant current density of 1 mA cm^{-2} using an electrochemical workstation (BioLogic SP-150 Potentiostat) in a two-electrode cell.

Electrochemical measurement. All electrochemical measurements were performed at room temperature using an electrochemical workstation (BioLogic SP-150 Potentiostat). A Pt foil served as the counter electrode and an Ag/AgCl electrode (saturated KCl) was used as the reference electrode. All potentials recorded against the Ag/AgCl reference electrode (without iR correction) were converted to the reversible hydrogen electrode (RHE) scale using the formula: $E_{RHE} = E_{Ag/AgCl} + 0.21\ V + 0.0591 * pH$, where pH represents the pH value of the solution. In the CO_2RR-fermentation hybrid cell, the cathode compartment was filled with 20 mL of 0.1 M glucose (0.5 M KCl), and the anode compartment contained 20 mL of 0.5 M $KHCO_3$ solution. The cathode and anode compartments were separated by a Nafion-117 membrane (Fuel Cell Store).

Product analysis. Gas products were analyzed using a GC (Trace 1310, Thermo Scientific) equipped with Molecular Sieve 5A and Porapak columns. Ar (Al Khafrah Industrial Gases, 99.999%) was used as carrier gas. CO, CH_4, C_2H_4 and C_2H_6 were quantified using a flame ionization detector (FID) with a methanizer. H_2 was quantified using a thermal conductivity detector (TCD). The volumes of the gas products were determined by analyzing the corresponding peak areas with reference to calibration curves. Liquid products were detected by a ^1H NMR spectrometer (Bruker, 600 MHz) employing the water suppression method. For each liquid sample, 480 μL of the electrolytes was mixed with 120 μL of internal standards, which consisted of 200 ppm of dimethyl sulfoxide (DMSO) in deuterium oxide (D_2O) and distilled water. Sorbitol was quantified using a Shimadzu Prominence HPLC system. A microtiter plate containing the collected samples was placed in the autosampler (SIL-20A) holder, and 2 mL of each sample was injected into the column (Shodex SP0810) for separation with water employed as the eluent. The column temperature was maintained at 30°C and the separated samples were detected using a refractive index detector (RID-10A). The Faradaic efficiency (FE) of a specific product (p) was calculated by the equation:

$$FE(p) = \frac{z * n * F}{Q} * 100(\%)$$

where z represents the number of the electrons transferred to one p molecule, n denotes the total moles of the product, F is the Faradaic constant (F = 96,485 $Cmol^{-1}$), and Q indicates the total number of electrons transferred.

Materials characterization and *In-situ* Raman characterization. X-ray powder diffraction (XRD) was carried out using Bruker D8 Advance with a Cu Kα radiation. HR-TEM and EELS images were imaged by

an aberration-corrected transmission electron microscope (TEM) of model Cs probe from ThermoFisher Scientific that was equipped with a post-column electron energy loss spectroscopy (EELS) equipment of model GIF-Quantum 966 from Gatan, Inc. The analysis was carried out by operating the microscope at an operating voltage of 300 kV.Scanning electron microscopy (SEM) images and energy-dispersive spectroscopy (EDS) were acquired using Teneo VS (Thermo Fisher – FEI) operated at 5 kV. XPS characterization were performed by a Kratos Analytical AMICUS/ESCA 3400 equipped with an Mg-anode Kα excitation X-ray source (hν = 1253.6 eV) at 10 kV, 10mA. Binding energies of the elements were referred to the C 1 s peak at 284.8 eV. *In-situ* Raman spectra were collected using a WITec apyron system equipped with a 633 nm laser beam and a water-immersion objective lens (Zeiss W Plan-Apochromat 63X/1) in a customized cell. To prevent laser-induced surface modification of the catalyst, a power of 30 mW was applied. In the customized *in-situ* Raman cell, a Pt wire served as the working electrode (CE), an Ag/AgCl electrode (saturated KCl solution) as the reference electrode (RE), and the cathode and anode compartments were separated by a Fumasep FKB-PK-130 membrane (Fuel Cell Store). Electrolyte (50 mL of 0.1 M glucose (0.5 M KCl)) were circulated to the cathode apartment at flow rates of 2 mL min^{-1}, respectively.

DFT calculation. The density function theory (DFT) calculations were implemented on Vienna Ab-initio Simulation Package (VASP) code[1, 2]. The interaction of core and electrons was treated by projector augmented wave (PAW) pseudopotential[3, 4] with a cut-off energy of 450 eV and the exchange-correlation function was described by the Perdew-Burke-Ernzerhof (PBE) method of the generalized gradient approximation (GGA)[5]. The Cu(111)-Ag(111) and Cu(111) were modeled to analyze the roles of interface of Cu-Ag, and 20 Ångström-thick vacuum layer was used to eliminate the interaction between two adjacent slabs. It is considered that geometry optimization is convergence the force of each atom less than 0.02 $eV \cdot Å^{-1}$. The DFT-D3(BJ) method was used to account for the vdW-dispersion energy-correction[6, 7]. The Brillouin zone was sampled on the Gamma centered Monkhorst-Pack (MP) grids[8], and the k-point was set to 3×3×1. The data processing was assisted by VASPKIT[9], QVASP[10] and VESTA[11] software. The Gibbs free energy difference (ΔG) between initial and final states was defined as[12, 13]:

$$\Delta G = \Delta E + \Delta ZPE - T\Delta S$$

Where E, ZPE, T and S represent the energy from DFT calculation, zero-point energy, temperature (298.15 K) and entropy, respectively.

TEA model

Our TEA follows the general outline set by literature[14-16]. We calculated the CO_2RR cost of producing 100 ton of ethanol per day with input data summarized in Table S1.

Table S1. Input data for TEA

Faradaic efficiency of ethanol	50%
Cell potential	2.5 V
Single pass conversion efficiency of CO_2	50%
Cost of CO_2	40 $*ton^{-1}

Cost of water	5 $*ton^{-1}
Cost of electrolyzer	304 $*kW^{-1}
Ethanol concentration	10%
Current density	0.5 A*cm^{-2}
Electricity cost	0.02 $*kWh^{-1}
CO_2 RR current density	0.2 A*cm^{-2}
Electrolyzer lifetime	20 years
Capital recovery factor	0.7
Plant capacity factor	0.9

Cost of electricity

$$Partial\ current\ (ethanol) = 100000\frac{Kg}{Day} * \frac{Day}{86400s} * 1000\frac{g}{Kg} * \frac{mol}{46g} * 12e^{-} * 96480\frac{C}{mol} = 29092488\ A$$;

$$Total\ current = \frac{Partial\ current}{Ethanol\ FE} = \frac{29092488\ A}{50\%} = 58184976\ A$$;

$$Electricity\ cost\ (\frac{\$}{ton\ ethanol}) = \frac{Consumed\ Power\ (kW)\ *\ 24\ hours\ *\ electricity\ price\left(\frac{\$}{kWh}\right)}{Ethanol\ yield\left(\frac{ton}{day}\right)} = \frac{\frac{58184976\ A * 2.5V}{1000}\ (kW)\ *\ 2}{100\ \left(\frac{ton}{day}\right.}$$

$$= 698.2\ \$/ton$$

.

Cost of eletrolyzer

We assumed the CapEx and OpEx of a CO_2 electrolyzer to be 304 $/kW based on the Hydrogen Analysis (H2A) production models[17]:

$$Electrolyzer\ cost\ (\$) = 304\frac{\$}{kW} * 0.2\frac{A}{cm^2} * 2.5V * \frac{kW}{1000W} * \frac{58184976A}{\frac{0.2A}{cm^2}} = 44220581.8\ \$$$;

Assuming no salvage value at the end of its lifetime (20 years), a capital recovery factor (CRF) based on a discount rate (i = 7%), and a plant capacity factor of 0.9, we have:

$$Electrolyzer\ cost\left(\frac{\$}{ton\ ethanol}\right)$$

$$= \frac{CRF_{electrolyzer} * Total\ electrolyzer\ cost}{Capacity\ factor * 365\frac{day}{year} * Production\ rate\ (\frac{100\ ton}{day})} = \frac{i * \frac{(1+i)^{lifetime}}{(1+i)^{lifetime}-1} * Tota}{Capacity\ factor * 365\frac{day}{year} * P}$$

$$= \frac{0.07 * \frac{(1+0.07)^{20}}{(1+0.07)^{20}-1} * \$44220581.8}{0.9 * 365\frac{day}{year} * 100\frac{ton}{day}} = 127.1\ \$/ton$$

.

Cost of CO_2

Assuming a 50% CO_2 single pass conversion efficiency and pressure swing adsorption (PSA) was used to recycle the residue CO_2.

For PSA, we used a reference cost of \$1989043 per 1000 m^3/h [18, 19] with a capacity scaling factor of 0.7 and OpEx consisting of only electricity at 0.25 kWh/m^3 [20]. We then have:

$$CO_2\ flow\ (per\ day) = 29092488\ A * \frac{1}{\frac{6\ e^-}{mol\ CO_2} * 96480\frac{C}{mol}} * 0.44\frac{kg}{mol} * \frac{86400s}{day} = 191055\ kg/day$$;

$$CO_2\ cost\left(\frac{\$}{ton\ ethanol)}\right) = \frac{191055\ kg}{100ton} * \frac{ton}{1000kg} * \frac{40\$}{ton} = 76.4\ \$/ton$$;

$$CO_2\ inlet\ flow = 191055\frac{kg}{day} * \frac{day}{24hr}\frac{1}{0.5} = 15921\ kg/hr$$;

$$CO_2\ outlet\ flow = \frac{15921kg}{hr} * \frac{1}{0.5} = 4020\frac{m^3}{hr}$$;

$$Hydrogen\ (byproduct)\ flow = 32324986 * (1-0.9)A * \frac{1}{2e^- * 96480\frac{C}{mol}} = 1446\frac{m^3}{hr}$$;

$$Total\ gas\ flow = 4020.5\frac{m^3}{hr} + 1446\frac{m^3}{hr} = 5466\frac{m^3}{hr}$$;

$$Total\ PSA\ capital\ cost = 1989043\ \$ * \left(\frac{5466}{1000}\right)^{0.7} = \$6531891$$;

$$PSA\ operation\ cost\left(\frac{\$}{ton\ ethanol)}\right) = \frac{0.25kWh}{m^3} * \frac{5466m^3}{0.5hr} * \frac{24hr}{day} * \frac{0.02\$}{kWh} * \frac{day}{100\ ton} = 6.6\ \$/ton$$;

Using the same method with electrolyzer cost:

$$PSA\ capital\ cost\left(\frac{\$}{ton\ ethanol}\right) = \frac{CRF_{PSA} * Total\ PSA\ cost}{Capacity\ factor * 365\frac{day}{year} * Production\ rate\ (\frac{100ton}{day})} = \frac{i * \frac{(1+i)^{lifetime}}{(1+i)^{lifetime}-1} *}{Capacity\ factor * 365\frac{day}{year} * P}$$

$$= \frac{0.07 * \frac{(1+0.07)^{20}}{(1+0.07)^{20}-1} * \$6531891}{0.9 * 365\frac{day}{year} * 100\frac{ton}{day}} = 18.8\ \$/ton$$

;

$CO_2\ cost\left(\frac{\$}{ton\ ethanol)}\right) = CO_2\ cost + PSA\ capital\ cost + PSA\ operation\ cost = 101.8\ \$/ton$.

Cost of ethanol distillation

Assuming the electrolyte effluent was recycled for an ethanol concentration of 10%:

$Ethanol\ flow\ rate = \frac{100000\ kg}{day} * \frac{5466\ m^3}{786\ kg} * \frac{day}{24hr} = 88\ L/min$;

$Electrolyte\ flow\ rate = \frac{88\ \frac{L}{min}}{0.1} = 880\ L/min$;

$Total\ distillation\ capital\ cost = \$4162240 * \left(\frac{880}{1000}\right)^{0.7} = \$3806444$;

$$Distillation\ capital\ cost\left(\frac{\$}{ton\ ethanol}\right) = \frac{CRF_{dis} * Total\ distillation\ capital\ cost}{Capacity\ factor * 365\frac{day}{year} * Production\ rate\ (\frac{100ton}{day})} = \frac{i * \frac{(1+i)^{lifetime}}{(1+i)^{lifetime}-1} * Total\ dist}{Capacity\ factor * 365\frac{day}{year} * Pro}$$

$$= \frac{0.07 * \frac{(1+0.07)^{20}}{(1+0.07)^{20}-1} * \$3806444}{0.9 * 365\frac{day}{year} * 100\frac{ton}{day}} = 10.9\ \$/ton$$

;

$Distillation\ operation\ cost\left(\frac{\$}{ton\ ethanol)}\right) = 9895\frac{\$}{day} * (\frac{880}{1000}) * \frac{day}{100\ ton} = 87.1\ \$/ton$;

$Ethanol\ distillation\left(\frac{\$}{ton\ ethanol)}\right) = Distillation\ capital\ cost + Distillation\ \ operation\ cost = 98\ \$/ton$.

Cost of water

Assuming no water can be recovered from the anode, we require 6 moles of water for every mole of ethanol produced:

$$Water\left(\frac{\$}{ton\ (ethanol)}\right) = \frac{18\frac{g}{mol}}{46\frac{g}{mol}} * 6 * \frac{5\ \$}{ton(H_2O)} = 11.7\ \$/ton$$

.

Cost of catalyst

We assume the one-time cost of catalyst is 5% of the electrolyzer cost and a lifetime of 5 years:

$$Catalyst\ and\ membrane\ cost\left(\frac{\$}{ton(ethanol)}\right) = \frac{CRF_{catalyst\ and\ membrane} * Total\ electrolyzer\ cost * 5\%}{Capacity\ factor * 365\frac{day}{year} * Production\ rate\ (\frac{100ton}{day})} =$$

$$\frac{i * \frac{(1+i)^{lifetime}}{(1+i)^{lifetime}-1} * Total\ electrolyzer\ cost * 5\%}{Capacity\ factor * 365\frac{day}{year} * Production\ rate\ (\frac{100ton}{day})}$$

$$= \frac{0.07 * \frac{(1+0.07)^5}{(1+0.07)^5-1} * 44220581.8\ \$ * 0.05}{0.9 * 365\frac{day}{year} * 100\frac{ton}{day}} = 16.4\ \$/ton$$

.

Cost of maintenance

We assume the cost of maintenance is 10% of electricity:

$$Maintenance\left(\frac{\$}{ton\ (ethanol)}\right) = 698.2 * 10\% = 69.8\ \$/ton$$

.

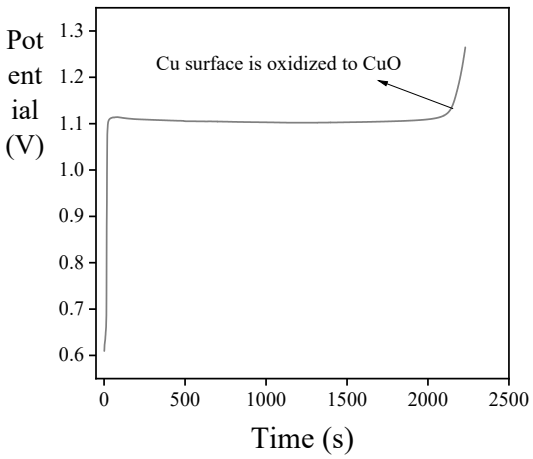

Fig. S1. The electrochemical oxidation of Cu at 1 mA cm^{-2} in 1 M NaOH solution.

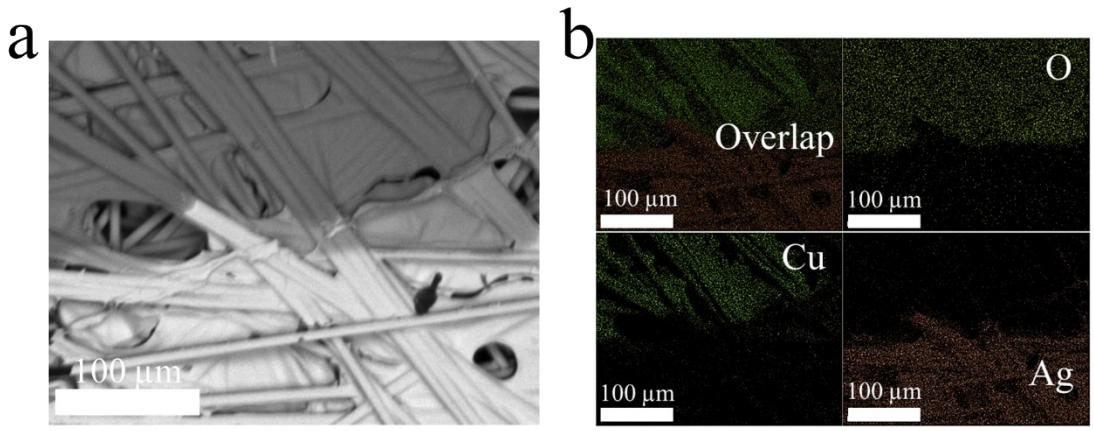

Fig. S2. (a) SEM and (b) EDS mappings of the CuO-Ag tandem electrode.

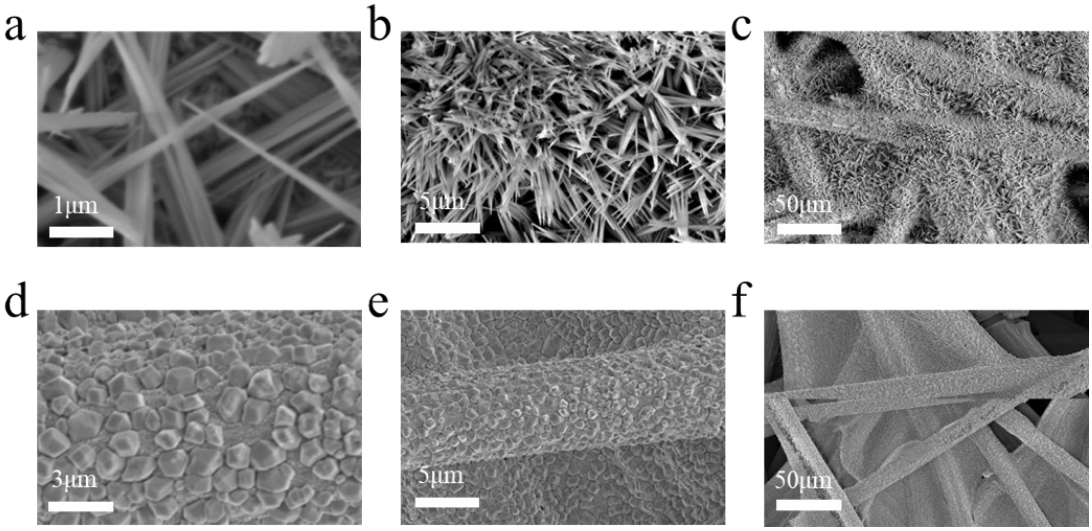

Fig. S3. SEM images of CuO nanoplates (a, b and c) and Ag nanoparticles (d, e and f).

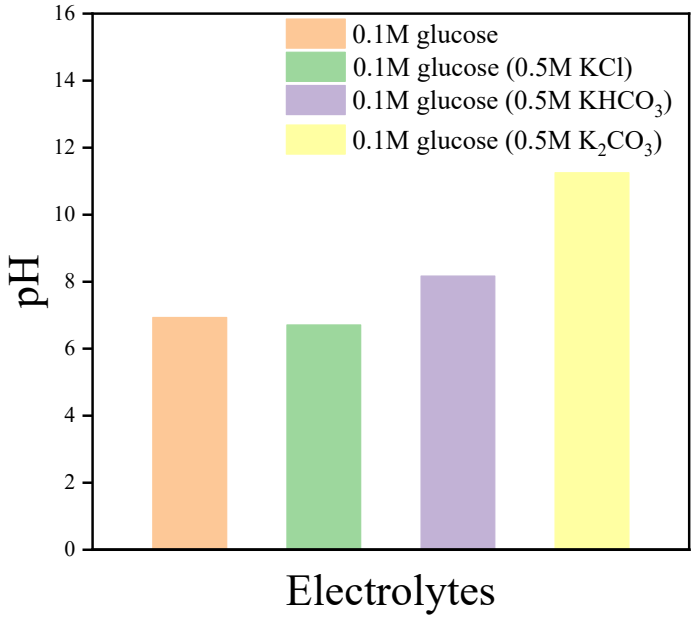

Fig. S4. pH of 0.1 M glucose solutions with different electrolytes.

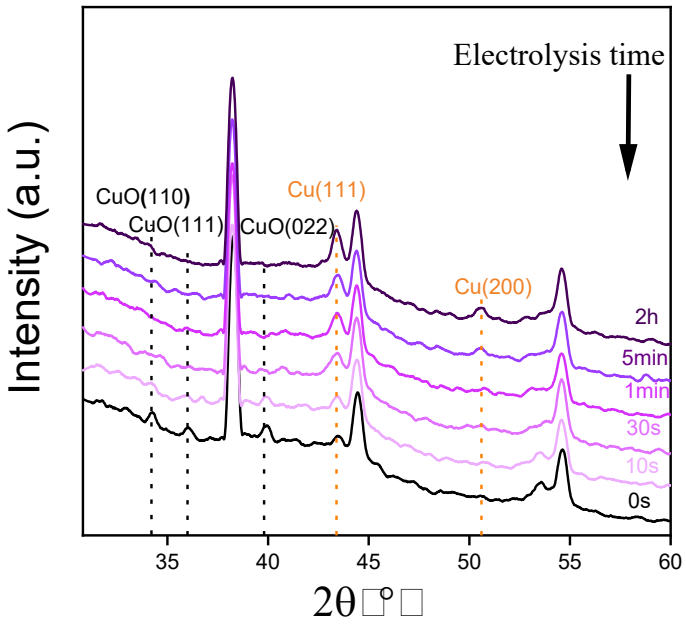

Fig. S5. Time-resolved XRD patterns of CuO-Ag (40) over 120 min of CO_2RR in 0.1 M glucose (0.5 M KCl) solution.

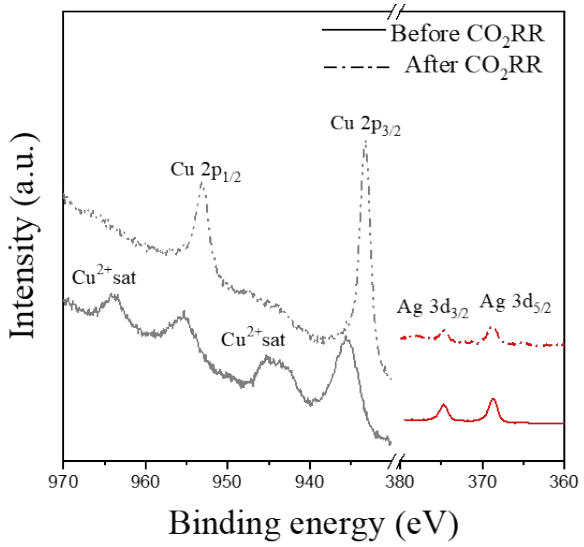

Fig. S6. XPS Cu 2p, Ag 3d spectroscopy before and after CO_2RR. The typical Cu 2p satellite peaks before CO_2RR indicates the characteristics of Cu^{2+} species, which proved the electrochemical oxidation of Cu to CuO[21]. No satellite peak was found after CO_2RR, suggesting that the original Cu^{2+} species are completely reduced after electrolysis. The Ag 3d peaks are located at 368 eV and 374 eV, which are consistent with the literature values of metallic Ag[22].

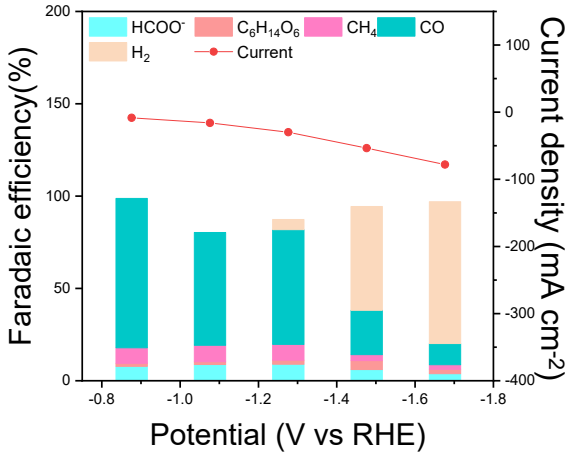

Fig. S7. FEs and current densities toward CO_2RR products, H_2 and sorbitol in 0.1 M glucose solution (0.5 M KCl) using Ag electrode.

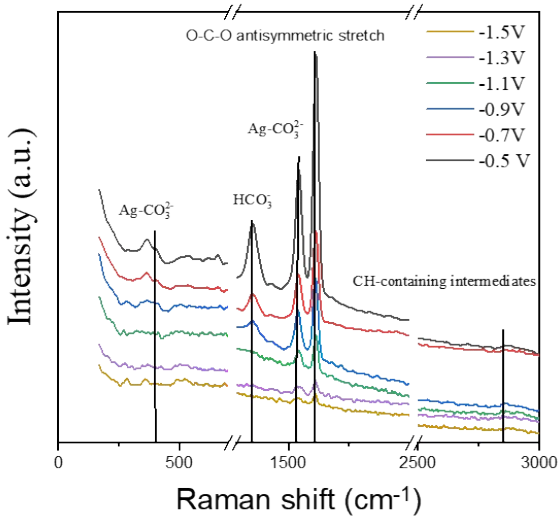

Fig. S8. *In-situ* Raman spectra acquired on Ag under different potentials (V vs RHE) in 0.1 M glucose (0.5 M KCl) solution. Specifically, the region of 396 cm^{-1} and 1500 cm^{-1} are identified as Ag-CO_3^{2-} bond, while the peak at 1625 cm^{-1} is assigned to anti-symmetrical stretching vibration of*CO2, which is consistent with reported literature[23-25].

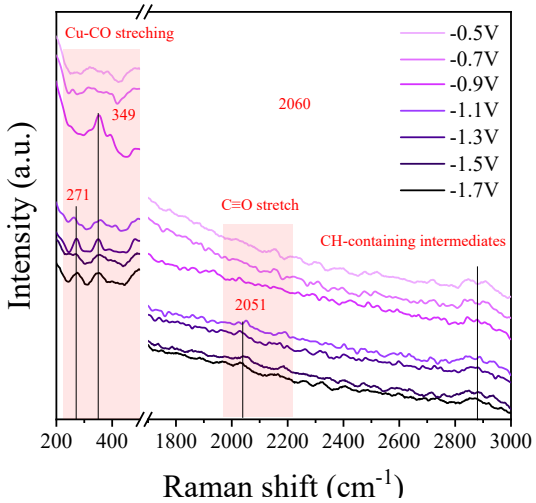

Fig. S9. *In-situ* Raman spectra acquired on CuO under different potentials (V vs RHE) in 0.1 M glucose (0.5 M KCl) solution.

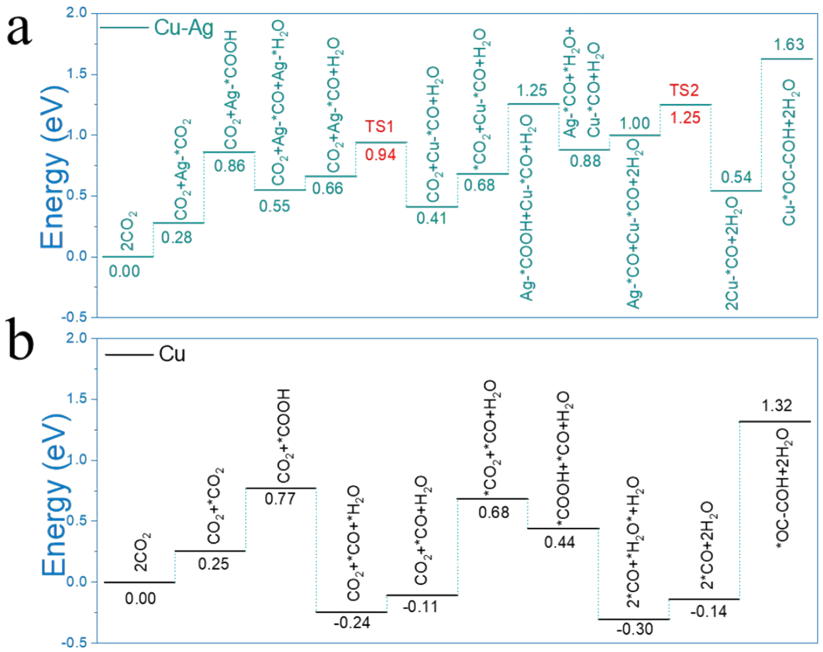

Fig. S10. Gibbs free energy diagram of CO_2RR process on (a) Cu-Ag interface and (b) bared Cu.

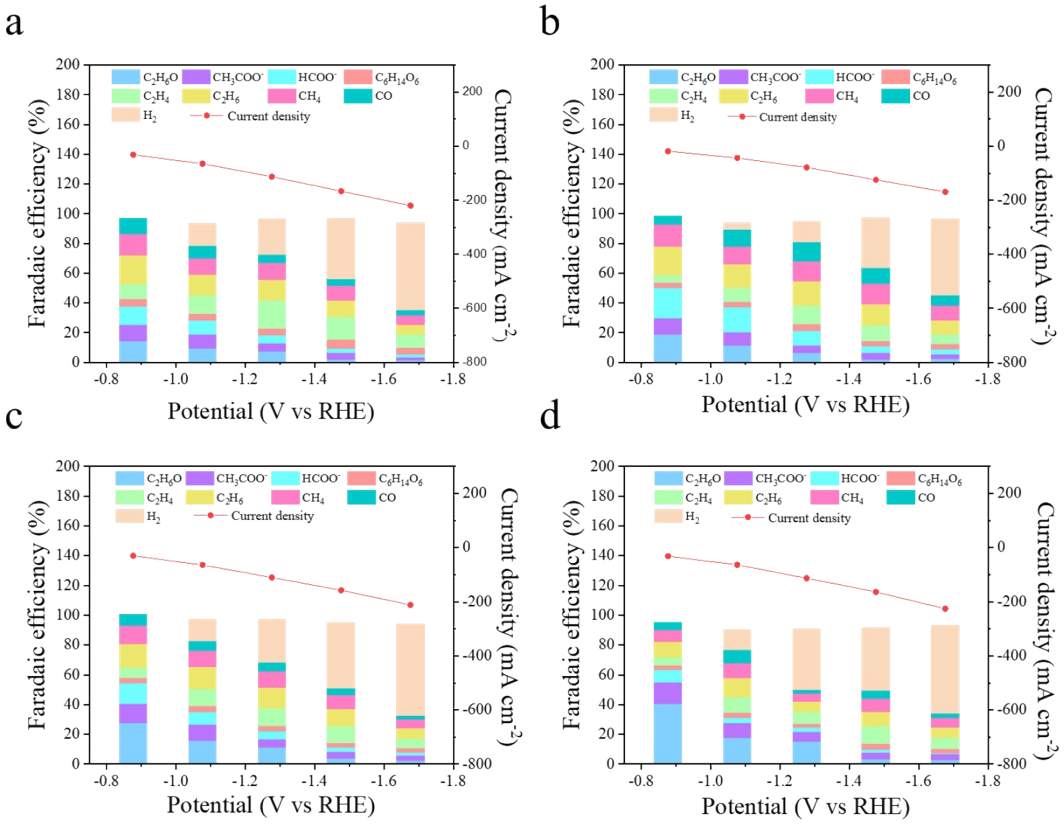

Fig. S11. FEs and current densities toward CO_2RR products, H_2 and sorbitol in 0.1 M glucose solution (0.5 M KCl) using (a) CuO electrode, and CuO-Ag tandem electrode with (b) 10, (c) 20 and (d) 30 interfaces.

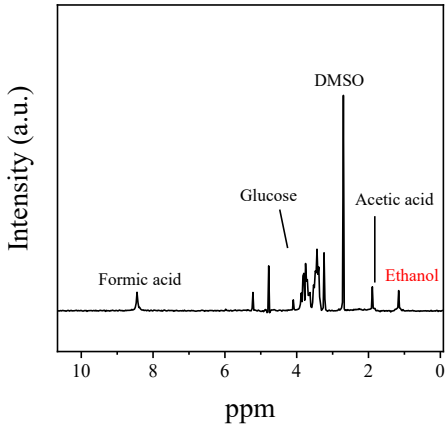

Fig. S12. NMR spectra of liquid products.

References

1. G. Kresse and J. Furthmüller, *Comput. Phys. Commun.*, 1996, **6**, 15-50.
2. G. Kresse and J. Furthmüller, *Phys. Rev. B*, 1996, **54**, 11169-11186.
3. G. Kresse and D. Joubert, *Phys. Rev. B*, 1999, **59**, 1758-1775.
4. P. E. Blöchl, *Phys. Rev. B*, 1994, **50**, 17953-17979.
5. J. P. Perdew, K. Burke and M. Ernzerhof, *Phys. Rev. Lett.*, 1996, **77**, 3865-3868.
6. S. Grimme, J. Antony, S. Ehrlich and H. Krieg, *The Journal of Chemical Physics*, 2010, **132**, 154104.
7. S. Grimme, S. Ehrlich and L. Goerigk, *J. Comput. Chem.*, 2011, **32**, 1456-1465.
8. D. J. Chadi and M. L. Cohen, *Phys. Rev. B*, 1973, **8**, 5747-5753.
9. V. Wang, N. Xu, J.-C. Liu, G. Tang and W.-T. Geng, *Comput. Phys. Commun.*, 2021, **267**, 108033.
10. W. Yi, G. Tang, X. Chen, B. Yang and X. Liu, *Comput. Phys. Commun.*, 2020, **257**, 107535.
11. K. Momma and F. Izumi, *J. Appl. Crystallogr.*, 2011, **44**, 1272-1276.
12. J. K. Nørskov, J. Rossmeisl, A. Logadottir, L. Lindqvist, J. R. Kitchin, T. Bligaard and H. Jónsson, *J. Phys. Chem. B*, 2004, **108**, 17886-17892.
13. J. Zhang, J. Ma, T. S. Choksi, D. Zhou, S. Han, Y.-F. Liao, H. B. Yang, D. Liu, Z. Zeng, W. Liu, X. Sun, T. Zhang and B. Liu, *J. Am. Chem. Soc.*, 2022, **144**, 2255-2263.
14. J. Sisler, S. Khan, A. H. Ip, M. W. Schreiber, S. A. Jaffer, E. R. Bobicki, C.-T. Dinh and E. H. Sargent, *ACS Energy Letters*, 2021, **6**, 997-1002.
15. H. Shin, K. U. Hansen and F. Jiao, *Nature Sustainability*, 2021, **4**, 911-919.
16. M. Jouny, W. Luc and F. Jiao, *Industrial & Engineering Chemistry Research*, 2018, **57**, 2165-2177.
17. D. Steward, T. Ramsden and J. Zuboy, *National Renewable Energy Laboratory (NREL)*, 2012.
18. M. Persson, O. Jönsson and A. Wellinger, 2006.
19. F. "Bauer, C. "Hulteberg, T. "Persson and D. "Tamm, *Biogas upgrading - Review of commercial technologies; Biogasuppgradering - Granskning av kommersiella tekniker*, ; Svenskt Gastekniskt Center (SGC), Malmoe (Sweden), Sweden, 2013.
20. A. Paturska, M. Repele and G. Bazbauers, *Energy Procedia*, 2015, **72**, 71-78.
21. W. Liu, P. Zhai, A. Li, B. Wei, K. Si, Y. Wei, X. Wang, G. Zhu, Q. Chen and X. Gu, *Nature Communications*, 2022, **13**, 1877.
22. D. Sun, P. Li, B. Yang, Y. Xu, J. Huang and Q. Li, *RSC advances*, 2016, **6**, 105940-105947.
23. X. Cao, D. Tan, B. Wulan, K. Hui, K. Hui and J. Zhang, *Small Methods*, 2021, **5**, 2100700.
24. Y. Ichinohe, T. Wadayama and A. Hatta, *Journal of Raman Spectroscopy*, 1995, **26**, 335-340.
25. K. G. Schmitt and A. A. Gewirth, *The Journal of Physical Chemistry C*, 2014, **118**, 17567-17576.